*Ab initio* study of oxygen vacancies in $BaTiO_3$



2000 J. Phys.: Condens. Matter 12 8239

(http://iopscience.iop.org/0953-8984/12/38/301)

J. Phys.: Condens. Matter **12** (2000) 8239–8247. Printed in the UK PII: S0953-8984(00)15610-3

# *Ab initio* study of oxygen vacancies in $BaTiO_3$

H Donnerberg and A Birkholz
University of Osnabrück, FB Physik, D-49069 Osnabrück, Germany

Received 19 July 2000

**Abstract.** In this paper we present embedded-cluster calculations on singly charged and neutral oxygen vacancies (or F centres) in the oxide perovskite $BaTiO_3$. The simulations include Hartree–Fock theory with MP2 corrections and density-functional-theory calculations for a central quantum defect cluster and a pair-potential description of the embedding lattice. All important defect-induced lattice distortions are taken into account in this way. We discuss the possible electronic states of charged F centres and the effects of nearby acceptor-type defects. It is shown that isolated oxygen vacancies induce electronic deep-gap levels. Scenarios are discussed to account for shallow-gap levels observed experimentally.

(Some figures in this article are in colour only in the electronic version; see `www.iop.org`)

## 1. Introduction

The major source of oxygen vacancies ($F^{++}$ centres or $V_O^{\bullet\bullet}$ in Kröger–Vink notation [1]) in oxide perovskites refers to charge compensations of acceptor-type impurity cations, which are always dissolved into these materials during crystal growth, with significant concentrations of the order of some hundreds of ppm. Thus, the same order of magnitude should be expected for F centres. Intrinsic defect reactions, on the other hand, are of only minor importance in this respect. Another effective source of oxygen vacancies relates to annealing treatments in reducing atmospheres. Here each oxygen vacancy created serves as a charge compensator of two electrons released to available electronic crystal states, i.e. to conduction band or donor-type defect states.

There are several reasons to investigate the properties of oxygen vacancies in oxide perovskites: oxygen vacancies represent donor-type defects which, in principle, are able to bind two electrons simultaneously. The trapping of one electron defines singly charged F centres ($F^+$), whereas two trapped electrons relate to neutral oxygen vacancies ($F^0$). Due to the estimated concentrations of such defects, one should expect significant influences on the observed n-type conductivity and on the optical absorption properties of the materials. This is of particular interest as regards moves towards a complete characterization of photorefractive material properties. In the present context it is important to study the favourable electronic states of electrons trapped at oxygen vacancies and to calculate the geometrical pattern of the resulting defect complexes.

Before discussing our embedded-cluster calculations, we review some of the recent experimental and theoretical investigations on oxygen vacancies.

The n-type conductivity of $BaTiO_3$ upon electrochemical reduction can be explained if oxygen vacancies are assumed to be completely ionized at elevated temperatures $T > 600\ ^\circ C$. This result indicates the existence of shallow-gap levels related to oxygen vacancies. However, to this day there is no proven structural model of these centres. Previous shell-model

0953-8984/00/388239+09$30.00  

simulations [2–4] suggested electronic ionization energies of about 0.1 eV. This agrees with recent experimental ionization energies (i.e. 0.2–0.3 eV [5]) which were derived from conductivity measurements. The shell-model estimate rests on the representation of $F^+$ centres as symmetry-broken $Ti^{3+}$–$V_O^{\bullet\bullet}$ defect complexes with the electron being localized at exactly one of the two Ti cations next to the vacancy; the electronic ionization energy has been obtained by combining shell-model defect energies with free-ion ionization potentials. Additional support in favour of this structural model seems to derive from empirical Green's function investigations [6–9]. However, it is emphasized that these latter results may be considerably modified upon changing the (empirical) model parametrizations. Moreover, these calculations do not include Ti 4s and 4p orbitals. Indeed, earlier discrete variational (DV) $X_\alpha$ cluster calculations [10] emphasized the importance of such additional orbitals accomplishing pronounced hybridizations between Ti $e_g(3d_{3z^2-r^2})$ (the $z$-axis corresponds to the main axis of the defect complex) and excited 4s and 4p orbitals. Another substantial point relates to the inclusion of vacancy-centred basis functions, which allow the transfer of electron density onto the vacant oxygen site. This obvious degree of freedom has been neglected completely in the earlier Green's function simulations, but has been accounted for in the present embedded-cluster calculations. The implications of these extensions, leading to substantial modifications of the structural model of oxygen vacancies, will be discussed below.

Recently Scharfschwerdt *et al* [11] published the details of careful electron spin-resonance investigations on paramagnetic defect centres observable in reduced $BaTiO_3$. The authors suggest interpretations in terms of $F^+$ centres assumed to consist of symmetry-broken $Ti^{3+}$–$V_O^{\bullet\bullet}$ defect complexes, as discussed above. Anticipating this interpretation, the investigations demonstrate the existence of two classes of $F^+$ centres, i.e. axial $Ti^{3+}$–$V_O^{\bullet\bullet}$ complexes orientated along $\langle 001 \rangle$ directions and non-axial centres, of which the $g$-tensor is moderately tilted against $\langle 001 \rangle$. For group-theoretical reasons the electronic ground state could be identified in both cases as Ti $t_{2g}(3d_{xy})$ which is orientated perpendicularly to [001]. In the case of non-axial centres the observed tilting has been ascribed to perturbing alkali acceptor cations incorporated at nearby Ba sites. Interestingly, only non-axial centres are observed if the $BaTiO_3$ samples are alkali contaminated. This indicates the importance of acceptor associations. The axial centres have been assigned to isolated oxygen vacancies. Finally, the $V_O^{\bullet\bullet}$-type centres have been contrasted successfully with isolated $Ti^{3+}$, representing a free small polaron in crystals containing $Nb^{5+}$ and no oxygen vacancies.

The present calculations are used to provide independent arguments concerning the microscopic structure of oxygen vacancies. The plan of this paper is as follows. First, we briefly review the embedded-cluster methodology which has been used throughout our investigations (section 2). In section 3 we present our calculated results and suggest a consistent theoretical model of oxygen vacancies in $BaTiO_3$. Due to their similarity with $BaTiO_3$, F centres in different oxide perovskites should behave analogously.

## 2. Simulation methods

The present real-space embedded-cluster calculations (ECC) are based on the extended 34-atom cluster $Ti_2O_{10}Ba_{12}Ti_{10}$ shown in figure 1, which correctly models the local mirror symmetry of the oxygen vacancy considered. The embedding lattice is simulated using a shell-model representation. All simulations are based on the cubic phase of $BaTiO_3$. This simplification may be justified by the observation that all possible ferroelectric distortions of the material are small compared with the usual defect-induced lattice relaxations.

The quantum mechanical description of the central defect cluster employs Gaussian-type basis functions with the split-valence quality for all titanium cations and oxygen anions inside

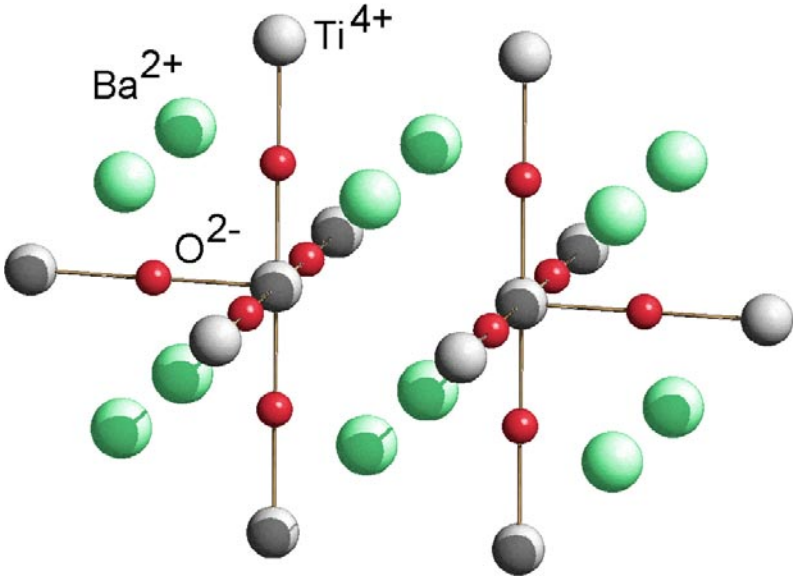


**Figure 1.** Visualization of the extended $Ti_2O_{10}Ba_{12}Ti_{10}$ cluster. The oxygen vacancy is located at the centre of this cluster; all further ion positions in this picture correspond to the undistorted cubic lattice structure of $BaTiO_3$.

the cluster; the oxygen basis set is augmented by polarizing d and diffuse p functions. Further, three s and three p-type basis functions with exponents 0.05, 0.1 and 1.0 have been implemented at the vacant oxygen site. The stability of these simulations has been investigated further by employing different sets of Gaussian basis functions for the central titanium cations, i.e. we used the HF-optimized set of Huzinaga *et al* [12] and the 3-21G set adapted for DFT-LDA calculations [13].

In all instances, bare effective core potentials (ECP) [14] have been used to model the localizing ion-size effects of all Ba and Ti cations at the cluster boundary. Similarly, occasionally associated acceptor impurity cations at Ba or Ti sites have been modelled by choosing appropriate ECP representations. In some instances we included the full electronic structure (implementation of 3-21G basis functions) of the associated acceptor.

The *ab initio* level of the present calculations covers Hartree–Fock (HF) theory including MP2 corrections and density-functional theory (DFT). All quantum cluster simulations have been performed on the basis of the quantum chemical CADPAC code [15]. Within DFT we used a generalized-gradient-approximation functional involving the Becke exchange term [16] and the correlation functional derived by Lee, Yang and Parr [17]. This exchange–correlation functional, abbreviated as 'BLYP', improves on the local-density approximation.

The modelling of the embedding lattice and of cluster–lattice interactions employs a shell-model pair-potential description (see also references [18–20]). The shell-model parameters have been taken from the earlier work of Lewis and Catlow [2]. It is noted that the shell model takes electronic polarization contributions of the embedding-lattice ions reasonably well into account. This feature is particularly important with respect to the highly polarizable oxygen anions. Figure 2 displays the embedding scheme. As in any classical Mott–Littleton defect calculation, the (embedding) crystal lattice is divided into three regions: region I which is explicitly equilibrated according to the underlying pair potentials, the interface region IIa and region IIb. Region II(a and b) is treated as a polarizable continuum using the harmonic

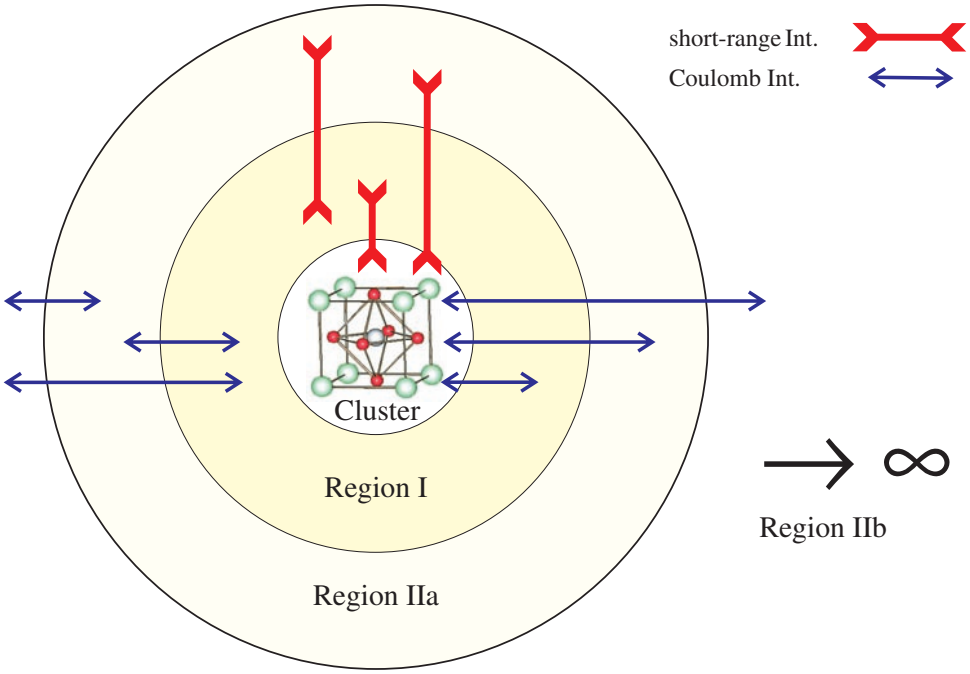


**Figure 2.** Visualization of the embedded-cluster calculations. The quantum cluster is embedded in a classically treated lattice consisting of the regions I, IIa and IIb. The arrows indicate the various existing interactions between the crystal regions.

approximation for the region-II self-energy. Whereas the interactions between the cluster and region I, on the one hand, and region IIa, on the other hand, are included explicitly, all region-IIb species feel only the effective defect charge of the central defect cluster. Details of this well-known description are given in reference [21]. All lattice calculations employ the CASCADE code [22].

The total energy of the complete model crystal is given by the expression

$$E(\rho, R_c, R_r) = \min_{\rho, R_c, R_r} \{E^{QM}_{Clust}(\rho, R_c) + E^{SM}_{Env}(R_r) + E^{Int}(\rho, R_c, R_r)\}. \qquad (1)$$

$\rho$, $R_c$ and $R_r$ denote the cluster electron density, the coordinates of the cluster nuclei and the positions of the shell-model species in the embedding environment, respectively. $E^{QM}_{Clust}$ represents the quantum mechanically calculated cluster self-energy, $E^{SM}_{Env}$ the Mott–Littleton-type shell-model energy of the embedding environment and $E^{Int}$ is the cluster–lattice interaction energy. The required minimization in equation (1) is performed using the programs CADPAC (variation of $\rho$ with fixed $R_r$) and CASCADE (variation of $R_r$ with fixed $R_c$ and $\rho$). In order to perform cluster geometry optimizations which are consistent with a predetermined embedding crystal lattice (represented by a point-charge field), an additional program has been written which updates the total cluster energies and gradients, as calculated by any quantum chemical program such as CADPAC, by adding the appropriate short-range pair-potential contributions due to the interactions between cluster ions and embedding-lattice species. With these updates, the program carries through the cluster geometry optimization using a variable-metric (quasi-Newton) minimization algorithm. The total minimization procedure is completed when the main cycle consisting of the alternating lattice- and cluster-equilibration subcycles converges.

It is finally noted that we have included a cluster electrostatic multipole consistency up to quadrupole order during the embedding-lattice relaxation step (see [23] for details). This is expected to be necessary due to a possible electronic charge transfer from cluster ions onto the vacant oxygen site, a situation which cannot be reasonably modelled within a formal-charge framework [24].

The present approach is designed to consistently integrate the local electronic structure and large-scale lattice-distortion effects, which are expected to be important in semi-ionic materials.

## 3. Results and discussion

As a starting model, we have considered the structure of isolated singly charged oxygen vacancies $F^+$. It is natural to assume that this model should display all main features known experimentally.

Figure 3 displays the calculated electron-density plots of a single electron trapped in Ti $e_g$ or in $t_{2g}$ states, alternatively. The notation for these states is adapted to the titanium site symmetry. To avoid $t_{2g}$ nodes, density contributions have been sampled above the $yz$-plane containing the central Ti–$V_O$–Ti complex. MP2 and DFT calculations consistently show that the $e_g$ state is about 1 eV more favourable than the shallow-gap $t_{2g}$ state†; even within the first-order HF approximation, the corresponding energy separation is 0.5 eV. Thus, seemingly at variance with experience, the calculations suggest a deep-gap ground-state level. Figure 3 indicates the occurrence of symmetry breaking only in the case of the $t_{2g}$ state, whereas the $e_g$ state relates to a highly symmetrical solution with the electron equally delocalized over the vacancy and both of its next Ti neighbours. Regarding the localized $t_{2g}$ state, we observed that lattice relaxation stabilizes the breaking of the symmetry. The calculations have also shown that the energetic preference of $e_g$ relates to hybridizations with excited Ti 4s and 4p orbitals and is further supported by the implementation of vacancy-centred orbitals. Only if we artificially omit these important degrees of freedom do we obtain a $t_{2g}$-type ground state—as in the empirical Green's function calculations mentioned earlier, in the introduction. Note that the $e_g$-state situation resembles proper $F^+$ centres, such as are known to exist in ionic alkali halides. In these centres, electrons are localized in s-type orbitals centred at the vacant anion site. In $BaTiO_3$ we observe a significant mixing between s-type vacancy orbitals and the neighbouring Ti $e_g(3d_{3z^2-r^2})$ states, which relates to the semi-ionic nature of this material.

The stability of the present embedded-cluster results, which are in good agreement with the earlier DV $X_\alpha$ cluster calculations of Tsukada *et al* [10], is impressive; in fact, they are qualitatively independent of the inclusion of lattice relaxations. Quantitatively, on allowing the lattice to relax, the energy separation between the $e_g$ and the $t_{2g}$ state increases by an amount of the order of 0.4 eV in favour of the $e_g$ state. This is seen consistently in all simulations that we have performed so far. Moreover, our important results favouring $e_g$-type ground states are not an artificial effect due to cutting off the electronic structure beyond the cluster surface within the embedded-cluster representation, but reflect physical reality. Independent FLMTO supercell calculations for F centres in $KNbO_3$ perovskites [25] as well as the recent supercell simulations of F centres in $PbTiO_3$ [26] provide additional strong support. Thus, from a theoretical point of view, we may conclude that properties of singly charged isolated oxygen vacancies are completely different from what is known experimentally. They cannot explain the main features of the corresponding ESR centres observed in reduced $BaTiO_3$. It is

† The ionization energy of this state amounts to a few tenths of an eV. It does not couple significantly with the environment, and the oxygen vacancy remains a perturbation.

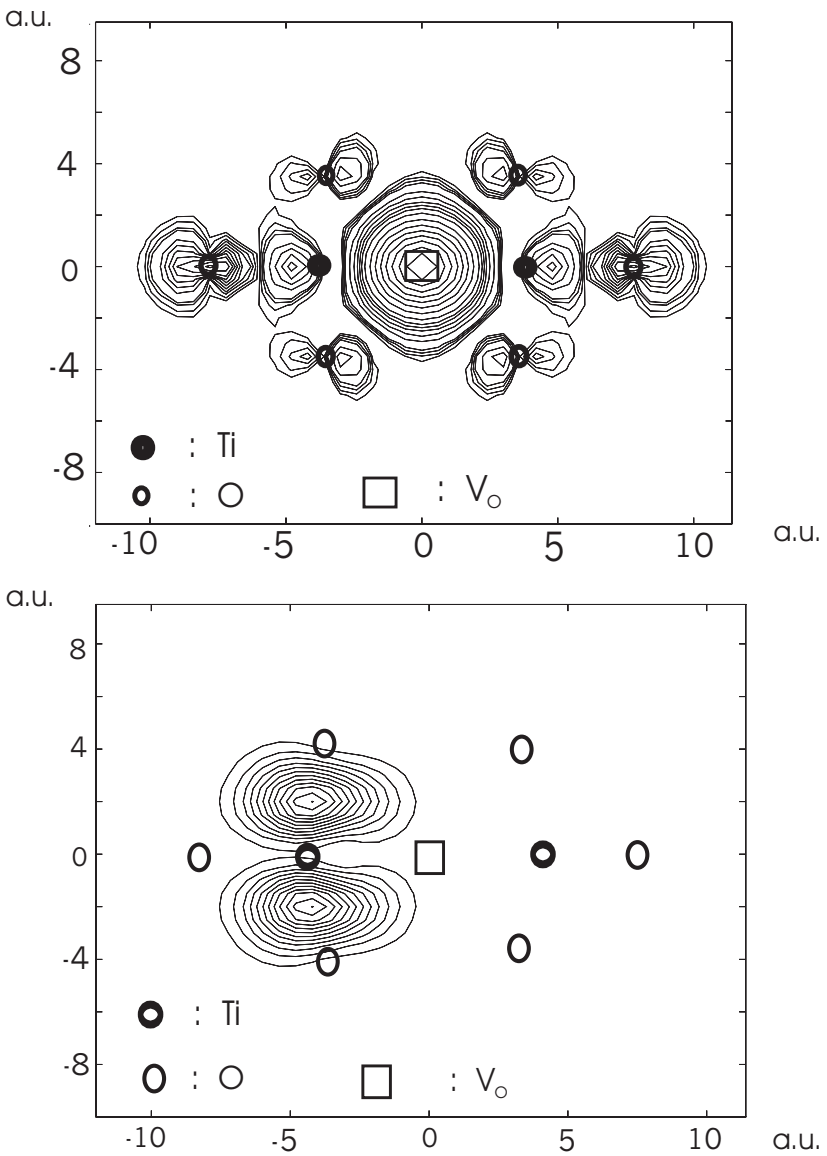


**Figure 3.** Visualization of the density of an electron trapped at an oxygen vacancy (upper picture: localization in an $e_g$ state; lower picture: localization in a $t_{2g}$ state). The results are obtained from ΔSCF calculations using DFT-BLYP.

finally recalled that electrons trapped in $e_g$-type orbitals would lead to significantly different ESR signals compared with the $t_{2g}$ situation. For example, due to vanishing coupling matrix elements, we should expect for the Zeeman-coupling $g$-value $g_\parallel \simeq g_e$ (for $\vec{z} \parallel \vec{B}$), i.e. the free-electron $g$-value. But this is decisively different from the observed value.

It is also of interest to consider the geometrical relaxation pattern of $F^+$ centres. Generally, our embedded-cluster calculations show that nearby oxygen anions become attracted towards the oxygen vacancy, whereas cations are repelled. In particular, neighbouring $Ti^{3+}$ cations are repelled by about 0.21 Å, if tacitly assumed in $t_{2g}$ states. However, this displacement vanishes

almost to zero if these cations are taken in their $e_g$-type ground states.

We are now in a position to speculate on model modifications towards consistent interpretations of the experimental data. What is the reason for the absence of ESR signals from isolated $e_g$-type $F^+$ centres in $BaTiO_3$?

As a first guess we could assume that all possibly existing isolated oxygen vacancies are used to form diamagnetic $F^0$ centres by trapping a second electron. This situation would correspond to a [100]-orientated electron bipolaron. The two spin-paired electrons would localize in $e_g$-type molecular orbitals. Though ESR silent, this hypothetical bipolaron should contribute specific observable optical absorption bands, which, however, have not been reported so far. Moreover, we should expect the formation of paramagnetic $e_g$-type $F^+$ centres upon modest heating of the crystal samples. Further, from theoretical simulations there are no unambiguous indications in favour of these centres. Probably these centres would dissociate spontaneously according to

$$F^0 + F^{++} \longrightarrow 2F^+. \tag{2}$$

In this sense, $F^0$ centres are expected to be of positive-$U$ type, with $U$ being of the order of 0.2 eV according to our embedded-cluster calculations at the DFT-BLYP level. In summary, a bipolaron-based explanation seems to be unlikely.

Next, we have discarded the existence of isolated oxygen vacancies in favour of acceptor-associated defect centres. Suitable acceptors not only reduce the symmetry to non-axiality, but could also suppress the formation of deep-gap $e_g$-type levels, leaving only the shallow-gap $t_{2g}$ states. In this context, acceptor cations are no longer considered as weak perturbations, but should strongly determine the electronic properties of oxygen vacancies. We emphasize that shell-model simulations predict the association of acceptor impurities at oxygen vacancies to be highly favourable. The precise energy of binding of oxygen vacancies to acceptor defects depends on the impurity's charge and size misfit. In the case of trivalent cations, the binding energies typically range between 0.3 and 0.5 eV. They are moderately smaller (i.e. 0.2 eV) for alkali impurities at Ba sites. Even two acceptors may be bound simultaneously with equal affinity. A complete saturation of oxygen vacancies with acceptor cations has also been postulated for fluorite-structured $MO_2$ oxides [2, 27]. For a majority of trivalent cations this would imply the association of two acceptor impurities simultaneously. Further indications towards acceptor association derive from ESR investigations in $BaTiO_3$ (see [11]).

Our embedded-cluster calculations suggest that Ba- and Ti-site acceptor cations associated one at a time are not effective in suppressing $e_g$ levels (see table 1). This result is due to acceptor-induced lattice relaxations, which effectively screen the misfit charge of the associated impurities: before lattice equilibration due to the additional acceptor, the negative acceptor charge of divalent and trivalent Ti-site acceptors suffices to suppress the $e_g$ state, being lowest. This result, however, is completely reversed in favour of the $e_g$ state if acceptor-induced lattice equilibration is allowed to take place. Also, it is just this screening of an acceptor misfit charge that causes the binding of a second acceptor to be as favourable as binding of the first acceptor. Finally, Ba-site acceptors are completely unable to suppress $e_g$ even before lattice relaxation. Thus, as a final model, we may conclude that only the simultaneous association of two Ti-site acceptors is able to inhibit the formation of deep-level $e_g$ states. In this hypothetical situation, conduction band electrons can localize only at second-neighbour Ti cations; the acceptor–vacancy complex remains a weak perturbation with respect to the cubic site symmetry of the second-neighbour Ti cation, and we thus expect a shallow-gap $t_{2g}$ ground state in agreement with currently available experimental information. Moreover, our preliminary simulations confirm that an electron forced to be trapped at a second-neighbour Ti cation localizes in a shallow-gap $t_{2g}$ state, being about 1 eV above the $e_g$ state relating to Ti cations nearest to

**Table 1.** Energy separation (at DFT-BLYP level) between $e_g$ and $t_{2g}$ states of oxygen vacancies associated with different acceptor impurities. The table also shows the effect of additional acceptor-induced lattice relaxations, which serve to screen the acceptor's charge misfit. P1–P3 denote the acceptor sites investigated, visualized in figure 4.

| | $E(e_g) - E(t_{2g})$ (eV) | |
|---|---|---|
| Acceptor | Without acceptor-induced GO | Including acceptor-induced GO |
| $Na^{+}_{Ba}$ (P1) | −0.2 | −0.8 |
| $Na^{+}_{Ba}$ (P2) | −0.15 | −0.3 |
| $Mg^{2+}_{Ti}$ (P3) | + 1.9 | −0.5 |
| $Al^{3+}_{Ti}$ (P3) | + 1.4 | −0.6 |
| $Sc^{3+}_{Ti}$ (P3) | + 1.1 | −0.8 |

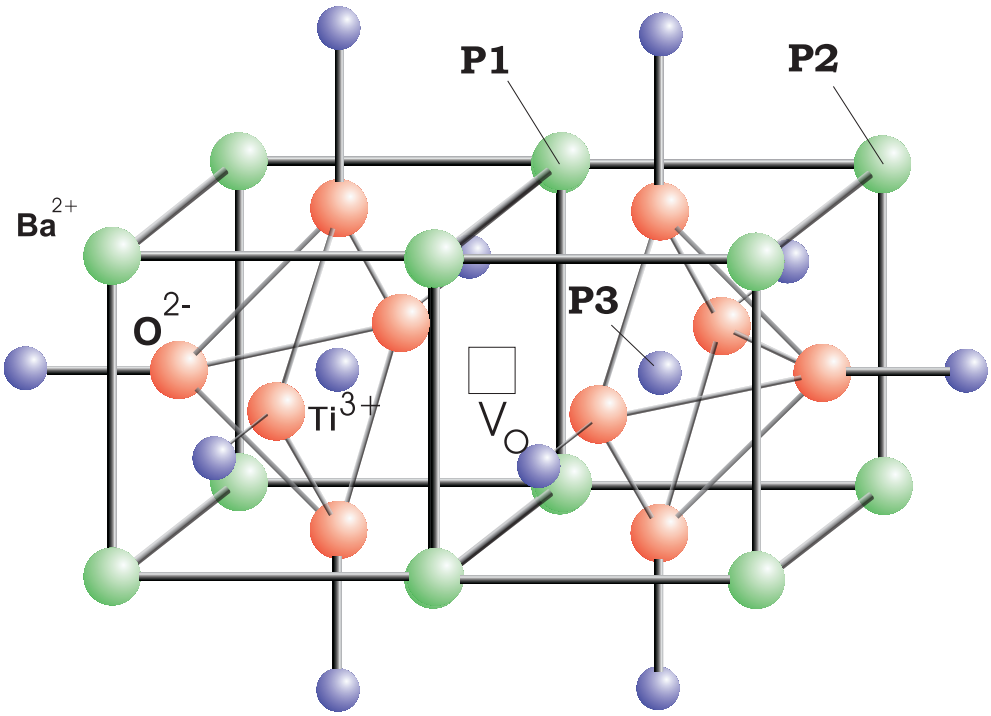


**Figure 4.** Visualization of the incorporation sites investigated for acceptor cations in barium titanate. The positions denoted by P1 and P2 refer to Ba sites, which are nearest and next nearest to the oxygen vacancy, respectively. P3 denotes a nearest Ti site.

the vacancy. The estimated ionization energy of this shallow-gap state is about 0.1 eV. A crucial experiment on this suggestive scenario consists of ESR measurements on extremely pure (i.e. acceptor-free) reduced $BaTiO_3$ crystals. Only then should we expect ESR signals of $F^{+}$ centres with electrons trapped in $e_g$ orbitals. Additional conductivity measurements would complete the proof.

## Acknowledgments

We gratefully acknowledge the financial support of this work by the Deutsche Forschungsgemeinschaft (SFB 225). We also thank Professor O F Schirmer for many valuable discussions.

## References

[1] Kröger F A and Vink H J 1956 *Solid State Physics* vol 3, ed F Seitz and D Turnbull (New York: Academic)
[2] Lewis G V and Catlow C R A 1986 *J. Phys. Chem. Solids* **47** 89
[3] Exner M, Catlow C R A, Donnerberg H and Schirmer O F 1994 *J. Phys.: Condens. Matter* **6** 3379
[4] Exner M 1993 *PhD Thesis* University of Osnabrück
[5] van Stevendaal U, Buse K, Kämper S, Hesse H and Krätzig E 1996 *Appl. Phys.* B **63** 315
[6] Selme M O and Pecheur P 1983 *J. Phys. C: Solid State Phys.* **16** 2559
[7] Fisenko A V, Prosandeyev S A and Sachenko V P 1986 *Phys. Status Solidi* b **137** 187
[8] Prosandeyev S A and Osipenko I A 1995 *Phys. Status Solidi* b **192** 37
[9] Prosandeyev S A, Fisenko A V, Riabchinski A I and Osipenko I A 1996 *J. Phys.: Condens. Matter* **8** 6705
[10] Tsukada M, Satoko C and Adachi H 1980 *J. Phys. Soc. Japan* **48** 200
[11] Scharfschwerdt R, Mazur A, Schirmer O F, Hesse H and Mendricks S 1996 *Phys. Rev.* B **54** 15 284
[12] Huzinaga S, Andzelm J, Klobukowski M, Radzio-Andzelm E, Sakai Y and Tatewaki H (ed) 1984 *Gaussian Basis Sets for Molecular Calculations* (Amsterdam: Elsevier)
[13] Andzelm J, Radzio E and Salahub D R 1985 *J. Comput. Chem.* **6** 520
[14] Hay W R and Wadt P J 1985 *J. Chem. Phys.* **82** 270
[15] Amos R D *et al* 1994 *Cambridge Analytic Derivatives Package (CADPAC)* version 5.2 (Cambridge University)
[16] Becke A D 1988 *Phys. Rev.* A **38** 3098
[17] Lee C, Yang W and Parr R G 1988 *Phys. Rev.* B **37** 785
[18] Donnerberg H and Bartram R H 1996 *J. Phys.: Condens. Matter* **8** 1687
[19] Donnerberg H and Birkholz A 1995 *J. Phys.: Condens. Matter* **7** 327
[20] Donnerberg H 1995 *J. Phys.: Condens. Matter* **7** L689
[21] Catlow C R A and Mackrodt W C (ed) 1982 *Computer Simulation of Solids (Springer Lecture Notes in Physics vol 166)* (Berlin: Springer)
[22] Leslie M 1983 *Solid State Ion.* **8** 243
[23] Vail J M, Harker A H, Harding J H and Saul P 1984 *J. Phys. C: Solid State Phys.* **17** 3401
[24] Donnerberg H, Többen S and Birkholz A 1997 *J. Phys.: Condens. Matter* **9** 6359
[25] Postnikov A V, private communication
[26] Park C H and Chadi D J 1998 *Phys. Rev.* B **57** R13 961
[27] Nowick A S and Park D S 1976 *Superior Conductors* (New York: Plenum)